ELSEVIER

Journal of Fluids and Structures 19 (2004) 123–140

JOURNAL OF FLUIDS AND STRUCTURES

www.elsevier.nl/locate/jnlabr/yjfls

Coupling of structure and wake oscillators in vortex-induced vibrations

M.L. Facchinetti[a,b], E. de Langre[a,*], F. Biolley[b]

[a] *Département de Mécanique, LadHyX-CNRS, Ecole Polytechnique, 91128 Palaiseau, France*
[b] *IFP-1,4 av. de Bois Préau, 92852 Rueil-Malmaison, France*

Received 5 August 2002; accepted 25 November 2003

Abstract

A class of low-order models for vortex-induced vibrations is analyzed. A classical van der Pol equation models the near wake dynamics describing the fluctuating nature of vortex shedding. This wake oscillator interacts with the equation of motion of a one degree-of-freedom structural oscillator and several types of linear coupling terms modelling the fluid–structure interaction are considered. The model dynamics is investigated analytically and discussed with regard to the choice of the coupling terms and the values of model parameters. Closed-form relations of the model response are derived and compared to experimental results on forced and free vortex-induced vibrations. This allows us to set the values of all model parameters, then leads to the choice of the most appropriate coupling model. A linear inertia force acting on the fluid is thus found to describe most of the features of vortex-induced vibration phenomenology, such as Griffin plots and lock-in domains.

1. Introduction

Vortex-induced vibrations (VIV) are a well-known phenomenon to engineers. Several kinds of structures subjected to wind or water currents may experience VIV: common posts, chimneys, suspended cables for bridges, power transmission lines in air, and pipes, risers, towing cables, mooring lines in water. In some cases, this has to be taken into account in their design as a potential cause of fatigue damage, such as for offshore structures.

Nominal two-dimensional (2-D) vortex shedding and consecutive VIV have been considered in earlier studies as the simplest form of the problem. Focusing onto crosswise VIV, phenomenological models have been developed in the 1970s following the idea of a wake oscillator (Birkoff and Zarantanello, 1957; Bishop and Hassan, 1964). The near wake dynamics was described by a single flow variable modelling the fluctuating nature of the vortex shedding. This variable was assumed to satisfy a van der Pol or Rayleigh equation which models a self-sustained, stable and nearly harmonic oscillation of finite amplitude. This elementary wake oscillator was naturally coupled with the motion equation of a one degree-of-freedom (1dof) elastically supported rigid structure, namely a structure oscillator. Some major features of the near wake vortex shedding and VIV have been thus qualitatively and quantitatively described, using analytical and numerical methods. For a comprehensive review see for instance Parkinson (1989).

Increasing computational resources have made possible the direct numerical simulation (DNS) of incompressible Navier–Stokes equations on 2-D domains around a fixed, forced or free structure profile: this has provided more detailed flow field analysis to compare with experimental observations.

Three-dimensional (3-D) features naturally arise in the VIV problem as the real domain is explicitly considered as spanwise extended: elastic structures like tensioned cables and beams are characterized by their eigenmodes, wake flows

*Corresponding author. Tel.: +33-1-69-33-36-01; fax: +33-1-69-33-30-30.
E-mail address: delangre@ladhyx.polytechnique.fr (E. de Langre).

0889-9746/$ - see front matter © 2003 Elsevier Ltd. All rights reserved.
doi:10.1016/j.jfluidstructs.2003.12.004

show secondary instabilities and the environment may impose shear flow. From a numerical point of view, computational limits arise for flow-field direct numerical simulation capability in modeling 3-D domains with large aspect ratio: simulations of VIV on flexible tensioned cables and beams have been performed for Reynolds number, Re, up to 10^3 and aspect ratio of about 10^3 (Lucor et al., 2001).

Phenomenological models based on wake oscillators may again be useful in describing such problems. Allowing accessible analytical considerations, they help in the understanding of the underlying physics. This explains several recent improvements in this approach. The original kernel in the form of van der Pol or Rayleigh equation has been re-interpreted by Balasubramanian and Skop (1997), Skop and Luo (2001), Krenk and Nielsen (1999), Mureithi et al. (2000) and Plaschko (2000), and then applied in its 3-D version. Wake oscillators have been continuously distributed along the spanwise extent of a slender structure and allowed to interact directly, in order to describe 3-D features of vortex shedding from stationary structures (Noack et al., 1991; Balasubramanian and Skop, 1996) and VIV of slender structures in uniform and shear flows (Balasubramanian et al., 2000; Facchinetti et al., 2001, 2002b; Kim and Perkins, 2002). Moreover, other low-order models have also been proposed in the literature for the 3-D wake dynamics behind stationary or vibrating (forced) slender structures, such as nonlinear circle map oscillators (Olinger, 1998) and the complex Ginzburg–Landau equation (Park and Redekopp, 1992; Albarède and Provansal, 1995; Monkewitz et al., 1996).

Considering this large variety there is definitely a need to have a critical analysis in terms of the fundamental behavior associated with the simplest forms of the model. In the present paper a class of low-order models for transverse VIV of 1 dof structures in stationary uniform flow is investigated. The basic van der Pol kernel is selected as a generic model (Section 2). In order to keep the model as simple as possible, only linear coupling terms for the fluid–structure interactions are considered. The model dynamics is investigated analytically and discussed with respect to the type of coupling and the value of its parameters. This allows us to compare the basic dynamics of old coupling models of the literature with the proposed new one, which considers a linear inertial action of the structure on the near wake. The constant values of all model parameters are first estimated from experimental data considering a forced wake oscillator, modelling the vortex shedding behind a structure whose movement is imposed (Section 3). The dynamical properties associated with the different coupling models are expressed in closed form and then compared for both forced and fully coupled wake and structure oscillators (Section 4). While the qualitative dynamics of the coupling models proposed by other authors is recovered from these solutions, a new linear inertial coupling is shown to be the most effective in describing, qualitatively and in some aspects quantitatively, the main features of 2-D VIV phenomenology. Discussion and conclusions are finally developed (Sections 5 and 6).

2. VIV model

2.1. Structure oscillator

Let us consider a 1 dof elastically supported rigid circular cylinder of diameter D, constrained to oscillate transversely to a stationary and uniform flow of free stream velocity U, Fig. 1. The dimensional in-plane cross-flow displacement Y

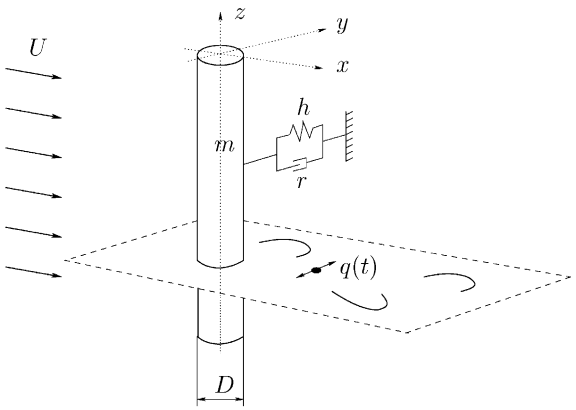

Fig. 1. Model of coupled structure and wake oscillators for 2-D vortex-induced vibrations.

of the structure is described by the linear oscillator

$$m\ddot{Y} + r\dot{Y} + hY = S \tag{1}$$

referred to as the structure oscillator in the sequel, where $(\cdot)$ means derivative with respect to the dimensional time T. The mass m takes into account both the mass of the structure m_s and the fluid-added mass m_f, which models inviscid inertial effects (Blevins, 1990), and reads

$$m = m_s + m_f, \quad m_f = C_M \rho D^2 \pi/4, \quad \mu = (m_s + m_f)/\rho D^2, \tag{2}$$

where the fluid density is ρ, μ is a dimensionless mass ratio and C_M is the added mass coefficient. In Eq. (1) the linear damping r models both viscous dissipations in the support r_s and the fluid-added damping r_f (Blevins, 1990), namely

$$r = r_s + r_f, \quad r_f = \gamma \Omega \rho D^2, \tag{3}$$

where γ is a stall parameter (see Balasubramanian and Skop, 1997; Skop and Luo, 2001) and Ω a reference angular frequency. In still fluid Ω is the angular frequency of the structure motion and γ is a function of the oscillation amplitude, related to the mean sectional drag coefficient of the structure C_D (Blevins, 1990). In our case of cross-flow Ω is the vortex-shedding angular frequency, $\Omega = \Omega_f = 2\pi \mathrm{St} U/D$, where St is the Strouhal number, and γ is again related to C_D (Blevins, 1990). For the sake of simplicity γ is here assumed to be a constant. This is equivalent to the model proposed by Balasubramanian and Skop (1997). In Eq. (1) the stiffness h only relates to external effects. In order to develop a 2-D model for VIV, all mass, damping and stiffness parameters are defined per unit length. Following Govardhan and Williamson (2000) hydrodynamic actions on the structure are here decomposed in two parts: the basic fluid effects, m_f and r_f, are directly included in the structure oscillator through m and r, Eqs. (2) and (3), while the effects of vortices are modelled by the right-hand side forcing term S, to be discussed later. Defining the structural angular frequency $\Omega_s = (h/m)^{0.5}$ and the structure reduced damping $\xi = r_s/(2m\Omega_s)$, Eq. (1) becomes

$$\ddot{Y} + \left(2\xi\Omega_s + \frac{\gamma}{\mu}\Omega_f\right)\dot{Y} + \Omega_s^2 Y = S/m. \tag{4}$$

2.2. Wake oscillator

The fluctuating nature of the vortex street is modelled by a nonlinear oscillator satisfying the van der Pol equation (Nayfeh, 1993)

$$\ddot{q} + \varepsilon\Omega_f(q^2 - 1)\dot{q} + \Omega_f^2 q = F \tag{5}$$

referred to as the wake oscillator in the sequel. The dimensionless wake variable q (Fig. 1) may be associated to the fluctuating lift coefficient on the structure, as for most of the models in the literature since the pioneering work of Hartlen and Currie (1970). It may alternatively be considered as a hidden flow variable related to a weighted average of the transverse component of the flow (Blevins, 1990), or assumed to be proportional to the transverse velocity of a representative near wake fluid mass (Krenk and Nielsen, 1999). It has also been associated to the mean transverse displacement of the local near wake fluid layer with respect to the mean streamwise axis (Noack et al., 1991). The right-hand side forcing term F models the effects of the cylinder motion on the near wake. When $F = 0$ and $0 < \varepsilon \ll 1$, the wake oscillator (5) is known to provide a stable quasi-harmonic oscillation of finite amplitude $q_o = 2$ at the angular frequency Ω_f (Nayfeh, 1993). Note here that considering a viscous term in the form $\varepsilon\Omega_f(\dot{q}^2 - 1)\dot{q}$, then referring to a Rayleigh equation as first proposed by Hartlen and Currie (1970), or a combination of both van der Pol and Rayleigh forms $\varepsilon\Omega_f(q^2 + \dot{q}^2 - 1)\dot{q}$ as considered by Krenk and Nielsen (1999), does not affect the capability of modelling a self-sustained stable quasi-harmonic oscillation of finite amplitude at the angular frequency Ω_f, namely a limit cycle in the phase portrait.

2.3. Coupling of wake and structure oscillators

Introducing the dimensionless time $t = T\Omega_f$ and space coordinate $y = Y/D$, Eqs. (4) and (5) lead to the coupled fluid–structure dynamical system

$$\ddot{y} + \left(2\xi\delta + \frac{\gamma}{\mu}\right)\dot{y} + \delta^2 y = s, \quad \ddot{q} + \varepsilon(q^2 - 1)\dot{q} + q = f, \tag{6}$$

where $\delta = \Omega_s/\Omega_f$ is the reduced angular frequency of the structure, also related to the reduced flow velocity U_r by

$$\delta = \frac{\Omega_s}{2\pi \mathrm{St}(U/D)} = \frac{1}{\mathrm{St}\,U_r}, \quad U_r = \frac{2\pi}{\Omega_s}\frac{U}{D} \tag{7}$$

and the dimensionless coupling terms read

$$s = \frac{S}{D\Omega_f^2 m} = S\frac{D}{4\pi^2\,\mathrm{St}^2\,U^2 m}, \quad f = \frac{F}{D\Omega_f^2} = F\frac{D}{4\pi^2\,\mathrm{St}^2\,U^2}. \tag{8}$$

Overdots now mean derivative with respect to the dimensionless time t. System (6) is the basic form of the phenomenological models of VIV using van der Pol oscillators, as considered in this paper. Several ideas have been proposed since Hartlen and Currie (1970), in order to model the fluid–structure coupling terms on the right-hand side. Adding nonlinearities on the left-hand side was also explored, as an attempt to match the model dynamical behavior with experimental results. For the most recent developments, see Balasubramanian and Skop (1997), Skop and Luo (2001), Krenk and Nielsen (1999), Mureithi et al. (2000), Plaschko (2000).

In order to keep the model as simple as possible, the fluid–structure coupling terms on the right-hand side are here limited to be linear functions of q and y and their time derivatives. No other nonlinearity is added in system (6), so that the only one is that of the van der Pol wake oscillator.

Since Hartlen and Currie (1970), the action s of the fluid near wake on the structure is usually considered as a fluctuating lift force. In dimensional variables, it reads

$$S = \tfrac{1}{2}\rho U^2 D C_L. \tag{9}$$

Note here that C_L does not correspond to the total instantaneous sectional lift coefficient on the structure because of S represents the forcing caused only by vorticity in the wake. Following Govardhan and Williamson (2000), in the sequel we will refer to C_L as the vortex lift coefficient and to C_L^{tot} as the total lift coefficient. The fluid variable q is then interpreted as a reduced vortex lift coefficient $q = 2C_L/C_{Lo}$, where the reference lift coefficient C_{Lo} is that observed on a fixed structure subjected to vortex shedding. The ratio $K = q/2 = C_L/C_{Lo}$ therefore describes the vortex lift magnification with respect to a fixed structure experiencing vortex shedding. In dimensionless form action (9) reads

$$s = Mq, \quad M = \frac{C_{Lo}}{2}\frac{1}{8\pi^2\mathrm{St}^2\mu}. \tag{10}$$

Since μ is a mass ratio, Eq. (2), M is essentially a mass number and scales the effect of the wake on the structure.

Conversely, several choices may be considered for the action f of the structure on the fluid wake oscillator. Hartlen and Currie (1970) have first taken "rather arbitrarily" (as stated in their original paper) a *velocity coupling* $f = A\dot{y}$, A being a parameter, as later assumed by Skop et al. (1973), Landl (1975), and more recently by Mureithi et al. (2000), Plaschko (2000). Krenk and Nielsen (1999) have suggested another model based on energy considerations: enforcing a direct flow of energy from the wake oscillator to the structure, in formulation (6) they derived a *displacement coupling* $f = Ay$. As a third choice, we propose here a linear inertial effect of the structure on the fluid, namely an *acceleration coupling* $f = A\ddot{y}$. The latter coupling has been previously considered in the literature, but only in combined models of VIV and galloping (see Parkinson, 1989; Blevins, 1990).

3. Values of model parameters

In this section all parameters of the class of models presented above are estimated through experimental data on free and forced vortex shedding behind cylinders. In order to compare the dynamical behavior of the three coupling models on a common basis, model parameters are fixed to the same constant values for the three coupling models.

In the dynamics of the structure oscillator, Eq. (6), the reduced damping ξ is a given parameter. The reduced frequency δ, Eq. (7), is also a given parameter that depends only on the Strouhal number St and the reduced velocity U_r. It is common practice to assume $\mathrm{St} = 0.2$ in the sub-critical range, $300 < \mathrm{Re} < 1.5 \times 10^5$ (Blevins, 1990; Pantazopoulos, 1994). Similarly, the mass ratio μ is directly derived from the structure and fluid masses, Eq. (2), assuming a constant-added mass coefficient C_M derived from potential flow theory (Blevins, 1990): in the case of a circular cross section it reads $C_M = 1$. The mass number M is then derived by Eq. (10). The reference lift coefficient C_{Lo} being usually taken as $C_{Lo} = 0.3$ in the large range of Re (Blevins, 1990; Pantazopoulos, 1994), using

(10) we therefore have

$$M = 0.05/\mu. \tag{11}$$

The only remaining parameter to be determined in the equation of the structure oscillator is the fluid-added damping coefficient γ, which is directly related to the mean sectional drag coefficient of the structure through (Blevins, 1990)

$$\gamma = \frac{C_D}{4\pi \mathrm{St}}. \tag{12}$$

For stationary cylinders in the sub-critical range, $300 < \mathrm{Re} < 1.5 \times 10^5$, we assume $C_{Do} = 1.2$ (Pantazopoulos, 1994). A drag magnification depending on the structure transverse motion may be taken into account in the form $(1 + 2y_o)C_{Do}$ (Blevins, 1990; Pantazopoulos, 1994), yielding a nonlinear term in the structure oscillator, but for the sake of simplicity we assume here a constant amplified drag coefficient $C_D = 2.0$, so that from Eq. (12)

$$\gamma = 0.8. \tag{13}$$

For the wake oscillator dynamics, Eq. (6), we only need to set values of the van der Pol parameter ε and the scaling of the coupling force f, namely A. This is done here by analyzing the effects of an imposed motion of the structure on the near wake dynamics. Experiments since those of Bishop and Hassan (1964) show that the lift force acting on the structure, namely q, is magnified by an imposed structure motion y, particularly at resonance. When the frequency of the forcing is close to the natural vortex shedding frequency, the vortex street deviates from Strouhal's law and synchronizes onto the forcing frequency, defining a lock-in state. Moreover, the phase shows an overall jump of about π when passing through lock-in, y and q being in-phase at low U_r and out-of-phase at high U_r, as confirmed by recent investigations on vortex shedding timing (Lu and Dalton, 1996; Carberry et al., 2001).

Considering an harmonic motion of dimensionless amplitude y_o and angular frequency ω, namely $y = y_o \cos(\omega t)$, the wake oscillator in (6) is forced by f which reads depending on the coupling model

$$f = Ay_o \cos(\omega t), \quad f = -A\omega y_o \sin(\omega t), \quad f = -A\omega^2 y_o \cos(\omega t), \tag{14}$$

in the case of displacement, velocity and acceleration coupling, respectively. Defining a reduced velocity based on the forcing frequency as

$$U_r = \frac{2\pi}{\omega \Omega_f}\frac{U}{D} = \frac{1}{\omega\,\mathrm{St}}, \tag{15}$$

the response of the wake oscillator is now analyzed for the three models of coupling in the parameter space (U_r, y_o). Enforcing the hypothesis of harmonicity and frequency synchronization, the response is sought in the form $q = q_o \cos(\omega t + \psi)$, where q_o and ψ are time-independent amplitude and phase, respectively. Substituting in the wake oscillator, Eq. (6), and considering only the main harmonic contribution of the nonlinearities, elementary algebra yields the amplitude of the transfer function of the wake oscillator

$$q_o^6 - 8q_o^4 + 16\left[1 + \left(\frac{\omega^2 - 1}{\varepsilon\omega}\right)^2\right]q_o^2 = 16\left(\frac{\|f\|}{\varepsilon\omega}\right)^2, \tag{16}$$

where $\|f\|$ is the amplitude of the forcing. Defining a reference lock-in state by $\omega = 1$ at $U_r = 1/\mathrm{St}$, Eq. (15), the vortex lift magnification factor with respect to a stationary structure experiencing vortex shedding, $K = q_o/2$, is derived as the unique real root of the bi-cubic polynomial of q_o, Eq. (16), and reads

$$K = \left(\frac{X}{36}\right)^{1/3} + \left(\frac{4}{3X}\right)^{1/3} \text{ with } X = \left(9\frac{A}{\varepsilon}y_o\right) + \sqrt{\left(9\frac{A}{\varepsilon}y_o\right)^2 - 48}. \tag{17}$$

In the literature, forced oscillation results are usually presented in terms of the total lift coefficient C_L^{tot}, which is related to the vortex lift coefficient C_L by the added mass effect

$$C_L^{\mathrm{tot}} = C_L - C_M 2\pi^3 \mathrm{St}^2 \ddot{y}, \tag{18}$$

so that for a harmonic evolution the total lift magnification factor K^{tot} reads

$$K^{\mathrm{tot}} = \sqrt{\left(K\cos\psi + \frac{C_M}{C_{Lo}}\frac{2\pi^3}{U_r^2}y_o\right)^2 + (K\sin\psi)^2}. \tag{19}$$

The particular choice of the coupling model does not affect the value of K because at the reference unitary angular frequency $\omega = 1$, so that in all cases we have $\|f\| = Ay_o$. Conversely, the relation between K^{tot} and K does depend on the phase ψ, and thus on the particular coupling model, as it will be discussed in the next section. In order to set

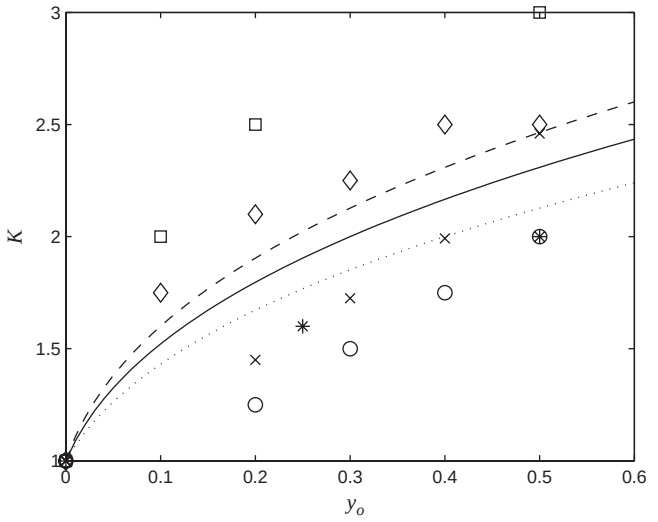

Fig. 2. Lift magnification K as a function of the imposed structure motion amplitude y_o. The model response (17) is fitted to experimental data: ♢, Vickery and Watkins (1962); ×, Bishop and Hassan (1964); ∗, King (1977); □, Griffin (1980); ○, Pantazopoulos (1994). Model parameters: ⋯, $A/\varepsilon = 30$; —, $A/\varepsilon = 40$ (proposed value); - -, $A/\varepsilon = 50$.

the value of the parameters ε and A once for all for the three coupling models, the approximation $C_L^{\text{tot}} \sim C_L$ is here applied. This implies a shift for the values of the parameters, but does not modify the basic dynamical behavior of the models: the comparison between them is thus made easier on a common basis. A further discussion on the value of ε and A is provided in Section 5.

Under this approximation, the value of the combined parameter A/ε is first derived by matching the model response (17) to experimental data on total lift magnification from the literature Vickery and Watkins (1962), Bishop and Hassan (1964), King (1977), Griffin (1980), Pantazopoulos (1994). The value of $A/\varepsilon = 40$ is proposed from a least-squares interpolation, Fig. 2. Note that at higher imposed structure motion amplitudes, $y_o > 0.5$, experiments show that the lift magnification K becomes a decreasing function of y_o (Vickery and Watkins, 1962; Bishop and Hassan, 1964; King, 1977; Griffin, 1980; Pantazopoulos, 1994). This occurs when y_o becomes too large with respect to the natural crosswise spacing of the near wake vortex street, as discussed in Saffman (1992). This feature may not be explicitly described by a van der Pol wake oscillator forced by the structure motion, as the amplitude of its stable limit cycle grows indefinitely as a function of the forcing amplitude. Note also that K might depend on other parameters than the structure oscillation amplitude and frequency, but this is not considered in our approach.

Let us now consider the influence of the structure oscillation amplitude on the extent of lock-in. At both low and high U_r, the response amplitude q_o, Eq. (16), is smaller than the amplitude of the natural limit cycle $q_o = 2$, so that $K < 1$. The free wake oscillator response, $\omega = 1, q_o = 2$, is then supposed to prevail on the forced response, defining a lock-out state. Looking for the $K = 1$ boundary from polynomial (16) in the (U_r, y_o) plane, the lock-in domains are represented for the three coupling models in Fig. 3. The velocity coupling model shows a lock-in domain almost symmetric with respect to the reference reduced velocity $U_r = 1/\text{St}$, whereas for displacement and acceleration the lock-in range extends at higher and lower U_r, respectively. The difference in the dynamical behavior is obviously due to the factor ω in $\|f\|$, Eq. (14). Keeping the ratio A/ε constant at the chosen value of $A/\varepsilon = 40$, the parameter ε and therefore A may now be chosen by matching the model response (16) to experimental data on lock-in extension in the literature, Stansby (1976), Blevins (1990), higher values of ε and A meaning a wider lock-in domain. The values $\varepsilon = 0.3$ and $A = 12$ may therefore be reasonably proposed for all the three coupling models (Fig. 3).

4. Dynamical behavior of the coupled model

In this section, the dynamical behavior of the coupled system is analyzed and its solutions are investigated in the scope of differentiating the influence of the choice of the coupling model. For the displacement and velocity couplings, some of the dynamics have been described in Krenk and Nielsen (1999) and Balasubramanian and Skop (1997), respectively. The parameters $M, \gamma, \varepsilon, A$ are fixed now at the values obtained in the previous section, namely $M = 0.05/\mu, \gamma = 0.8, \varepsilon = 0.3, A = 12$.

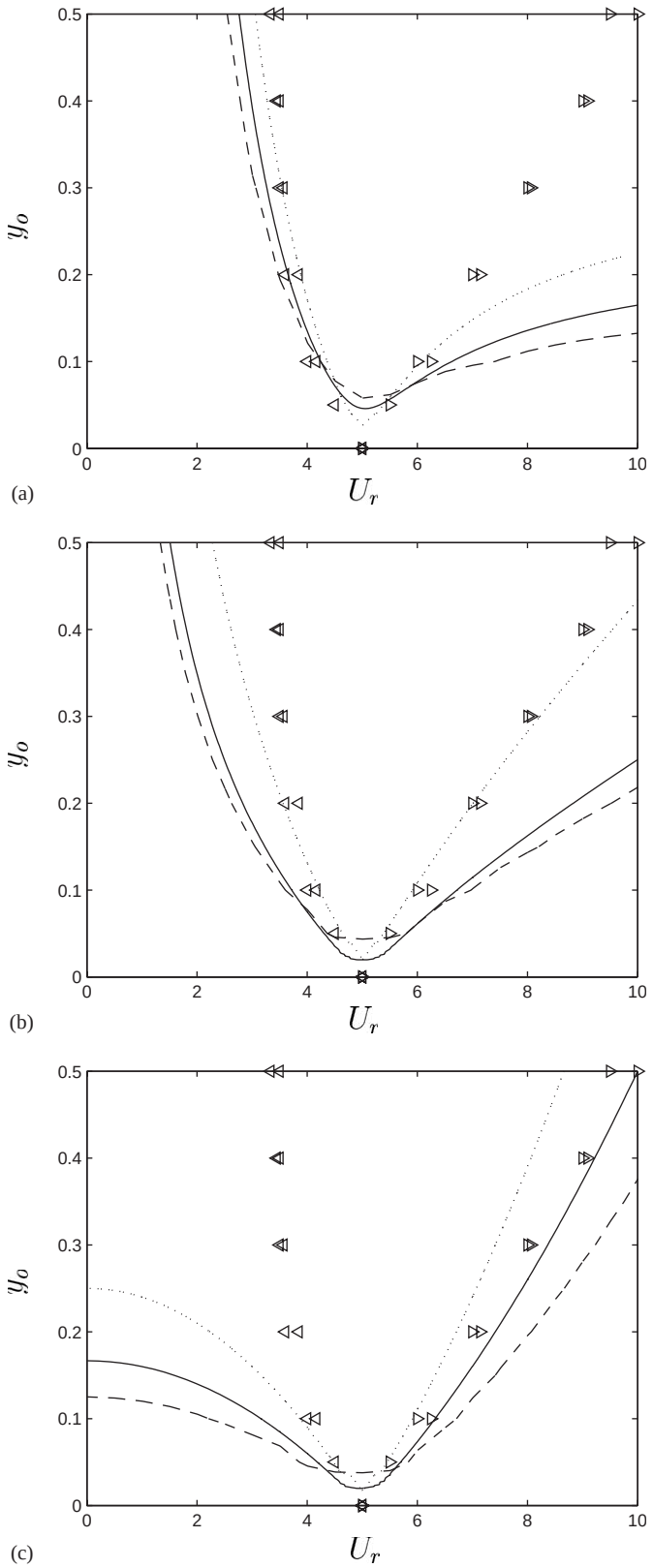

Fig. 3. Lock-in domain in the (U_r, y_o) plane looking for $K = 1$ boundary in the polynomial (16) for the different coupling models: (a) displacement; (b) velocity; (c) acceleration. Experimental data: $\triangleleft$, $\triangleright$, Stansby (1976), Blevins (1990). Model parameters: $\cdots$, $\varepsilon = 0.2$; —, $\varepsilon = 0.3$ (proposed value); - -, $\varepsilon = 0.4$.

4.1. Forced wake oscillator

Let us first come back to the case of an imposed motion of the structure on the near wake dynamics, i.e., to forced vortex shedding as in the preceding section. The phase of the transfer function of the wake oscillator may be analytically derived as for its amplitude counterpart (16) and reads

$$\psi = \theta, \quad \psi = \theta + \frac{\pi}{2} \tag{20}$$

with

$$\tan\theta = \frac{\varepsilon\omega}{\omega^2 - 1}\left(\frac{q_o^2}{4} - 1\right) \tag{21}$$

for the displacement, velocity and acceleration coupling models, respectively. In Fig. 4 it appears that the acceleration model seems more effective in describing the phase between the imposed structure motion and the fluctuating lift as observed in experiments (Bishop and Hassan, 1964; Bearman, 1984; Carberry et al., 2001): y and q are found to be in-phase at low U_r and out-of-phase at high U_r.

4.2. Coupled system

Let us now consider the coupled fluid–structure system given by (6). To the leading order, a solution is sought in the form

$$y(t) = y_o\cos(\omega t), \quad q(t) = q_o\cos(\omega t - \varphi), \tag{22}$$

where the structure and fluid signals admit time-independent common angular frequency ω, amplitudes q_o, y_o and relative phase φ. Substitution in the structure oscillator equation yields the amplitude and phase of the linear transfer function between the structure displacement and the fluid variable

$$\frac{y_o}{q_o} = M[(\delta^2 - \omega^2)^2 + (2\xi\delta + \gamma/\mu)^2\omega^2]^{-0.5}, \quad \tan\varphi = \frac{-(2\xi\delta + \gamma/\mu)\omega}{\delta^2 - \omega^2}. \tag{23}$$

Substituting now in the wake oscillator equation and considering only the main harmonic contribution of the nonlinearities, elementary algebra finally yields two equations on the amplitude q_o and the angular frequency ω

$$q_o = 2\left[1 + \frac{AM}{\varepsilon}\frac{C}{(\delta^2 - \omega^2)^2 + (2\xi\delta + \gamma/\mu)^2\omega^2}\right]^{0.5}, \tag{24}$$

$$\omega^6 - [1 + 2\delta^2 - (2\xi\delta + \gamma/\mu)^2]\omega^4 - [-2\delta^2 + (2\xi\delta + \gamma/\mu)^2 - \delta^4]\omega^2 - \delta^4 + G = 0, \tag{25}$$

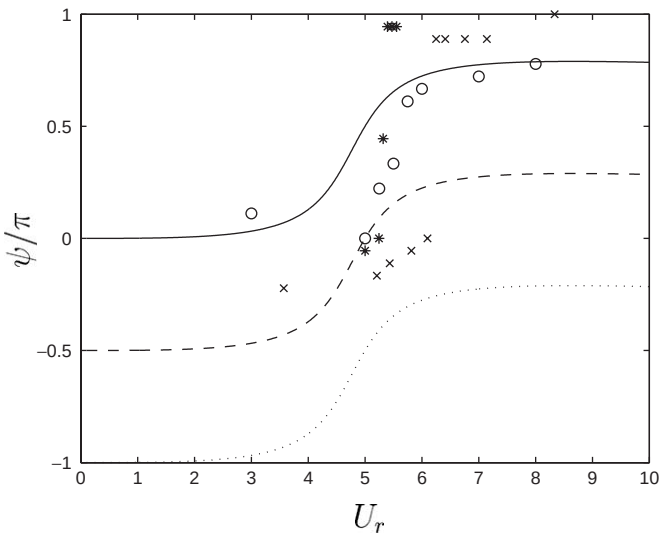

Fig. 4. Phase of q with respect to y as a function of U_r, Eq. (20), for the different coupling models: ⋯, displacement; - -, velocity; —, acceleration. Experimental data: ∗, Bishop and Hassan (1964); ×, Carberry et al. (2001); ○, Bearman (1984).

where the coefficients C and G depend on the particular coupling model f. For the displacement coupling it reads

$$C = -(2\xi\delta + \gamma/\mu), \quad G = AM(\delta^2 - \omega^2) \tag{26}$$

for the velocity coupling

$$C = \delta^2 - \omega^2, \quad G = AM(2\xi\delta + \gamma/\mu)\omega^2 \tag{27}$$

and for the acceleration coupling

$$C = (2\xi\delta + \gamma/\mu)\omega^2, \quad G = AM(\omega^2 - \delta^2)\omega^2. \tag{28}$$

The angular frequency ω directly arises as a solution of the bi-cubic equations (25), yielding one or three positive real roots. The amplitudes y_o, q_o and the relative phase φ then derive accordingly, via Eqs. (24) and (23), respectively. Distinct roots are associated to hysteretic behavior. We may now explore these various solutions depending on the particular choice of the coupling models, when the reduced velocity is varied. In order to illustrate this, we shall consider the case of a uniform pivoted cylinder experiencing transverse VIV in uniform flow (Balasubramanian et al., 2000), for which $\xi = 3.1 \times 10^{-3}$, $M = 2 \times 10^{-4}$. In order to assess the stability of all solutions, the dynamical system (6) has been numerically treated by standard centered finite difference in time and integrated by a second order accurate time explicit scheme.

Let us first consider the appearance of the lock-in phenomenon which we define here as a deviation of the wake and structure common frequency ω from Strouhal law, namely $\omega = 1$. For all the three models of coupling, the system angular frequency resulting from (25) is found to be locked onto the structure angular frequency $\omega = \delta = 1/(\mathrm{St}\, U_r)$ around $U_r = 1/\mathrm{St}$ (Fig. 5). Actually, the basic resonance state $\omega = 1 = \delta$ for which $U_r = 1/\mathrm{St}$ is not an exact solution for the velocity coupling, as it is for displacement and acceleration models. Out of lock-in, the coupled system is synchronized onto the vortex shedding angular frequency $\omega = 1$. For the acceleration coupling, hysteretic behavior occurs at both lock-in boundaries, whereas for displacement and velocity models the whole lock-in domain is characterized by hysteresis. Moreover, for displacement and acceleration couplings, lock-in is nearly symmetric with respect to a reference resonance slightly higher than $U_r = 1/\mathrm{St}$. Conversely, the dynamical response of the velocity model is asymmetric: the unique lock-in branch develops only at reduced velocities higher than $U_r = 1/\mathrm{St}$, while at lower reduced velocities there exist only lock-out states.

Let us now consider the amplitude y_o of the structure motion, derived from the frequency solutions ω using Eqs. (24) and (23) (Fig. 6). For all the three coupling models, the lock-in condition is found to yield a magnification of the structure motion, whereas at lock-out the structure is almost at rest, $y_o \ll 1$. The displacement coupling model displays a very weak motion amplitude even at lock-in, at least of an order of magnitude less than those of velocity and acceleration coupling models. Moreover, the displacement coupling model shows two independent lock-in branches, as

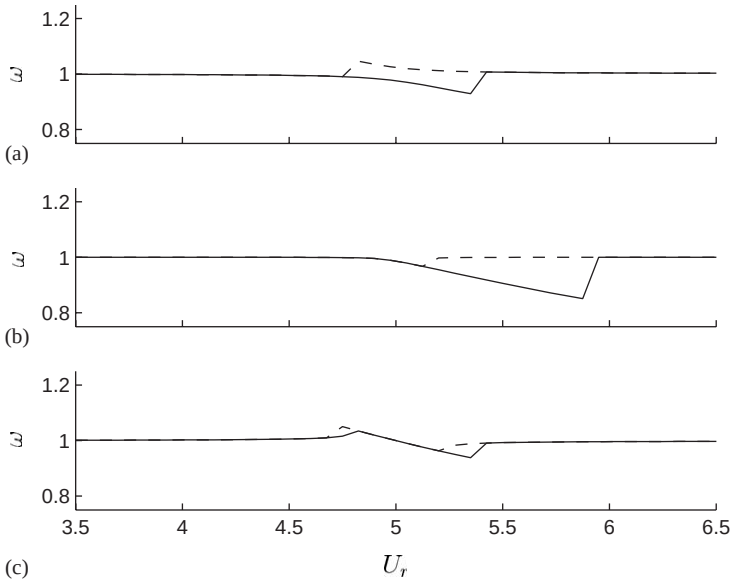

Fig. 5. Angular frequency ω as a function of reduced velocity U_r: (a) displacement model; (b) velocity model; (c) acceleration model. —, increasing U_r; - -, decreasing U_r.

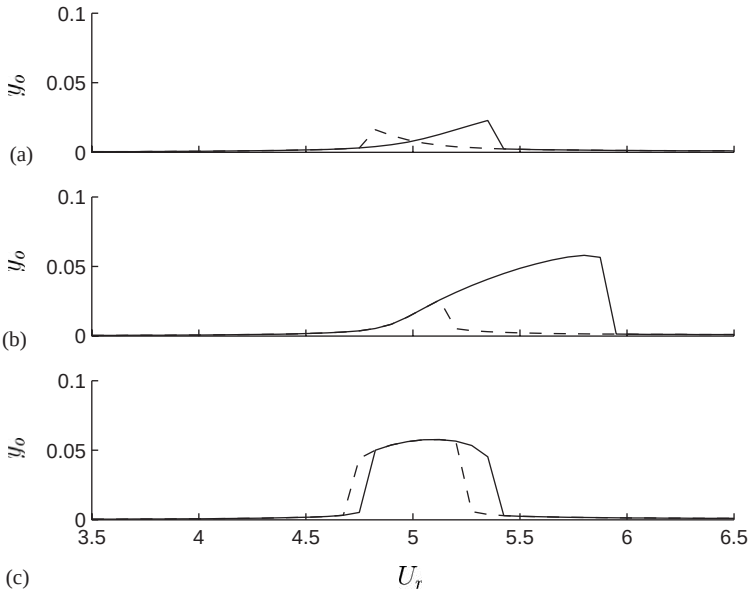

Fig. 6. Amplitude of the structure oscillator y_o as a function of reduced velocity U_r: (a) displacement model; (b) velocity model; (c) acceleration model. —, increasing U_r; - -, decreasing U_r.

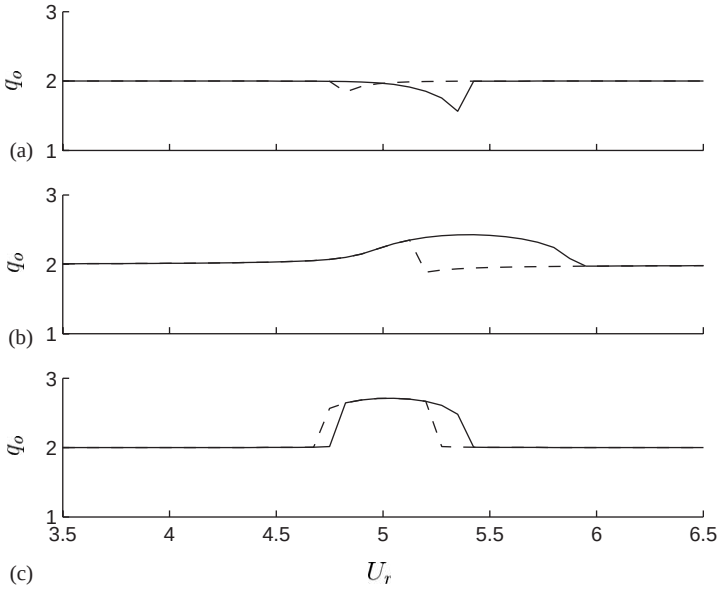

Fig. 7. Amplitude of the wake oscillator q_o as a function of reduced velocity U_r: (a) displacement model; (b) velocity model; (c) acceleration model. —, increasing U_r; - -, decreasing U_r.

may also be seen in Krenk and Nielsen (1999), which are not a simple prolongation of a common resonance kernel around $U_r = 1/\mathrm{St}$, as it is for velocity and accelerations couplings.

Considering now the wake variable amplitude q_o (Fig. 7), the displacement coupling model does not succeed in describing the lift magnification during lock-in. In fact, as noted by Krenk and Nielsen (1999), this coupled system is adiabatic: an increase of the structure oscillation amplitude is allowed only by a decrease in the wake oscillation amplitude. Conversely, for velocity and acceleration couplings, a lift magnification is observed. Out of lock-in, system (6) simply models vortex shedding from a stationary structure: the wake oscillator sets itself on the limit cycle of amplitude $q_o = 2$, the structure being almost at rest, $y_o \ll 1$, see Fig. 6.

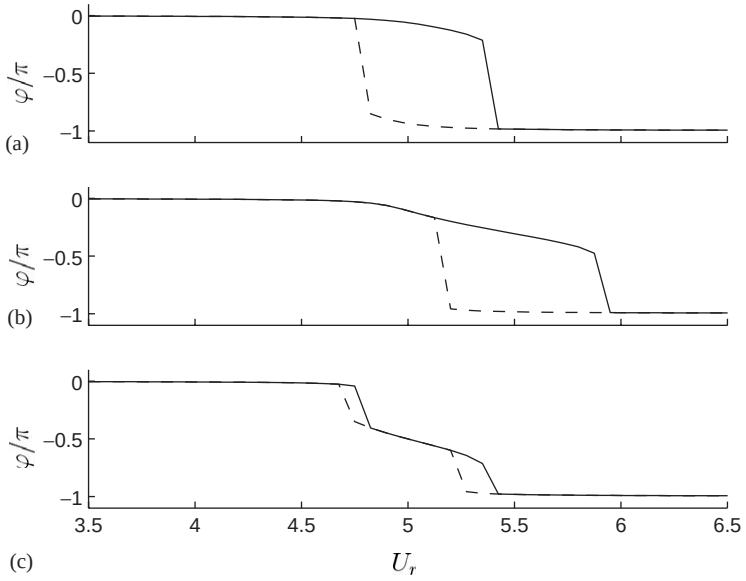

Fig. 8. Phase φ between structure and wake oscillators as a function of reduced velocity U_r: (a) displacement model; (b) velocity model; (c) acceleration model. —, increasing U_r; - -, decreasing U_r.

For all the three coupling models the phase φ between the structure and wake oscillators, Eq. (23), shows an overall phase jump of π passing through lock-in, Fig. 8. This is qualitatively consistent with results in the literature concerning the change in vortex shedding timing that occurs when passing through the lock-in domain (Khalak and Williamson, 1999; Govardhan and Williamson, 2000; Carberry et al., 2001). Actually, the jump in the lift phase observed in experiments is very abrupt, for both forced and freely vibrating structure. This later feature is not well represented by the acceleration coupling model, which shows a phase jump at both lock-in boundaries.

Considering the results of Figs. 5–8 on the dynamics of the coupled system (6) when U_r is varied, we may now say that the displacement coupling model fails in describing two major features of lock-in, namely large structure oscillation and lift magnification, whereas the velocity and acceleration coupling models yield results that differ between them, namely concerning the location of the lock-in domain, but are both qualitatively consistent with experimental data.

4.3. Oscillation amplitude at lock-in

The maximum structure displacement amplitude at lock-in is typically expressed in the literature as a function of a single combined mass-damping parameter, namely the Skop–Griffin parameter S_G,

$$S_G = 8\pi^2 \,\mathrm{St}^2 \,\mu\xi = \frac{C_{Lo}}{2}\frac{\xi}{M}, \tag{29}$$

yielding the so-called Griffin plot (Khalak and Williamson, 1999). Let us now derive an explicit relation between the maximum structure displacement amplitude and S_G for the coupled system (6), to be compared to experimental data.

For the displacement coupling model, the reference resonance state defined by $\omega = \delta = 1$ at $U_r = 1/\mathrm{St}$ satisfies polynomial (25) but it is not exactly associated to the maximum structure displacement amplitude, see Fig. 6a. Nevertheless, this provides a qualitative information on the system dynamical behavior at lock-in. Combining Eqs. (23), (24) and (29) yields the structure displacement amplitude at $\omega = \delta = 1$

$$y_M = \frac{C_{Lo}/2}{S_G + 4\pi^2 \mathrm{St}^2 \gamma}\sqrt{1 - \frac{A}{\varepsilon}\frac{C_{Lo}/4}{S_G + 4\pi^2\,\mathrm{St}^2\,\gamma}}. \tag{30}$$

The lift magnification factor with respect to the case of vortex shedding from a stationary structure, $K_M = q_M/2$, correspondingly reads

$$K_M = \sqrt{1 - \frac{A}{\varepsilon}\frac{C_{Lo}/4}{S_G + 4\pi^2\,\mathrm{St}^2\,\gamma}}. \tag{31}$$

As observed previously in this section, the displacement model does not succeed in describing the lift magnification during lock-in, see also Fig. 7a. The lift magnification factor K_M is always smaller than one and is even not defined when S_G is smaller than the critical value

$$(S_G)_c = \frac{A}{\varepsilon}\frac{C_{Lo}}{4} - 4\pi^2 \mathrm{St}^2\gamma = 1.7. \tag{32}$$

Eqs. (30) and (31) provide real positive amplitudes y_M and K_M for $S_G > (S_G)_c$ only. For smaller values of S_G, the reference resonance state $\omega = \delta = 1$ is not allowed and the basic resonance between structure and wake oscillators is suppressed. In this case, system (6) simply models vortex shedding as from a stationary structure: the wake oscillator sets itself on the limit cycle of amplitude $q_o = 2$ and frequency $\omega = 1$, as in the absence of any forcing, and the structure is almost at rest, $y_o \ll 1$. In terms of Griffin plot (Fig. 9), the displacement coupling model clearly fails to qualitatively match experimental data.

For the velocity coupling model, the maximum structural displacement amplitude is located almost at the upper U_r boundary of the lock-in domain, which corresponds to the exact solution $\omega = \delta_M \neq 1$, see Fig. 5b. Solving (25) under this condition yields

$$S_G\delta_M^3 + (4\pi^2\,\mathrm{St}^2\,\gamma)\delta_M^2 - S_G\delta_M - \left(4\pi^2\,\mathrm{St}^2\,\gamma - A\frac{C_{Lo}}{4}\right) = 0. \tag{33}$$

The corresponding structure oscillation amplitude y_M and the lift magnification factor K_M arise from (23) and (24) as

$$K_M = 1, \quad y_M = \frac{AC_{Lo}}{2(S_G\delta_M + 4\pi^2\,\mathrm{St}^2\,\gamma)\delta_M}. \tag{34}$$

The Griffin plot derived from the velocity coupling model (Fig. 9) is found to underestimate the structure oscillation amplitude, when using the values of parameters proposed in the preceding section. Yet, the qualitative influence of the Skop–Griffin parameter is recovered. Particularly, the asymptotic self-limited response amplitude at low S_G is assured by the fluid damping γ.

For the acceleration coupling model a reference resonance state is defined by $\omega = \delta = 1$ at $U_r = 1/\mathrm{St}$. It satisfies the frequency equation (25) and yields almost the maximum structure displacement amplitude, as previously shown in Fig. 6c, even if the maximum occurs at a value of U_r slightly higher than $1/\mathrm{St}$. Combining Eqs. (23), (24) and (29), the structure displacement amplitude at $\omega = \delta = 1$ reads

$$y_M = \frac{C_{Lo}/2}{S_G + 4\pi^2\,\mathrm{St}^2\,\gamma}\sqrt{1 + \frac{A}{\varepsilon}\frac{C_{Lo}/4}{S_G + 4\pi^2\,\mathrm{St}^2\,\gamma}}. \tag{35}$$

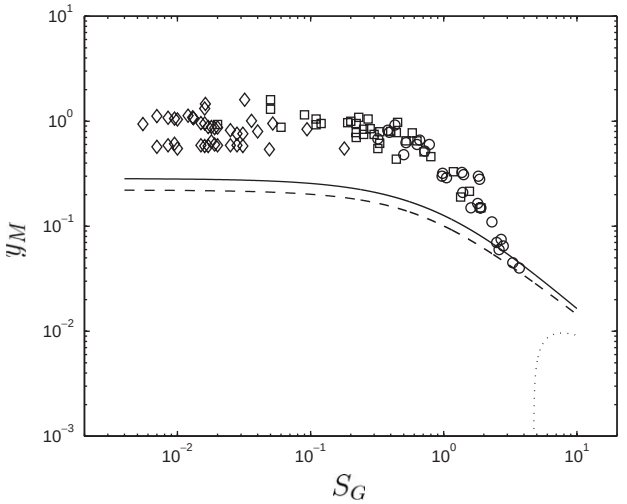

Fig. 9. Structural oscillation amplitude at lock-in y_M as a function of the Skop–Griffin parameter S_G: ···, displacement model; - -, velocity model; —, acceleration model. Experimental data in air: ○, Balasubramanian and Skop (1997). Experimental data in water: □, Balasubramanian and Skop (1997); ◇, Khalak and Williamson (1999).

The lift magnification factor K_M correspondingly reads

$$K_M = \sqrt{1 + \frac{A}{\varepsilon} \frac{C_{Lo}/4}{S_G + 4\pi^2 \mathrm{St}^2 \gamma}}. \tag{36}$$

In terms of Griffin plot (Fig. 9) this yields results similar to the velocity coupling model.

We may therefore state that, as in the preceding section, the displacement coupling model fails in describing even qualitatively the trend of experimental data of the Griffin plots, whereas the velocity and acceleration coupling models yield similar results, qualitatively consistent with experiments.

4.4. Extension of lock-in

Although the maximum structure displacement y_M and the corresponding lift magnification factor K_M at lock-in are determined by the single combined mass-damping parameter S_G, as verified for the three coupling models in the previous section, the range of lock-in is known to be a function of both $M(\mu)$ and ξ separately (Govardhan and Williamson, 2000). At low values of the mass-damping parameter, $S_G = 0.01$, the model dynamical behavior is now discussed in terms of the recent investigations of Govardhan and Williamson (2000). Another analysis on particular limits in the case of vanishing stiffness may be found in Leonard and Roshko (2001) and Shiels et al. (2001).

The lock-in domain is here considered at a constant S_G value as a function of the mass ratio $M(\mu)$ only, which is rewritten for the sake of comparison with the literature as

$$m^* = \frac{4}{\pi}\mu - C_M = \frac{0.2}{\pi M} - C_M. \tag{37}$$

Experiments show the existence of a critical mass ratio $m_c^* = 0.54$, under which large structure oscillation persists for high reduced velocities, at least to the limits of experimental facilities, and the oscillation frequency increases indefinitely with the flow velocity, meaning unbounded lock-in domain at higher U_r.

Let us define the range of lock-in, at given values of m^* and S_G, by an oscillation amplitude threshold, namely $y_o(U_r) > y_M/2$, where the maximum amplitude y_M is given in the preceding section. For the displacement coupling model, the lock-in state is simply defined by $y_o > 0.04$, as y_M is not defined for low S_G values. The extension of the lock-in domain as a function of U_r and m^* is derived and plotted in Fig. 10 for the three coupling models, respectively. For the displacement coupling model, Fig. 10a, as m^* tends to zero a constant structure oscillation amplitude persists at high U_r. Note that amplitudes are not really of significant magnitude and as $S_G < (S_G)_c$, Eq. (32), no real positive oscillation amplitudes are allowed around $U_r = 1/\mathrm{St}$. The velocity coupling model, Fig. 10b shows a lock-in domain that enlarges only to a finite reduced velocity range, as m^* tends to zero. Conversely, for the acceleration coupling model, Fig. 10c, as m^* tends to zero the widening of the lock-in domain is clearly unbounded and significant structure oscillations persist at high U_r. This latter result is quite consistent with experimental data of Govardhan and Williamson (2000).

It appears that, in terms of extension of lock-in, the three models yield quite different results, particularly at low mass ratio. In this range, only the acceleration coupling model is able to describe the phenomenon of persistent lock-in. This is illustrated in Fig. 11a by plotting the structural oscillation amplitude y_o as a function of the reduced velocity U_r, at a value of $m^* = 0.52$ lower than the critical mass ratio $m_c^* = 0.54$ found by Govardhan and Williamson (2000). For the displacement coupling model, a lock-out zone exists around $U_r = 1/\mathrm{St}$ as we have here $S_G < (S_G)_c$: this is clearly inconsistent with experiments. For the velocity coupling model, as observed by Hartlen and Currie (1970), the computed response sharply decreases after the maximum is reached. Only the acceleration coupling model is found to follow the trend of experiments. This is further confirmed by the evolution of frequency in Fig. 11b, where the results of the acceleration coupling model are consistent with experimental data. For the sake of comparison, the dimensionless frequency $f^* = \omega/\delta$ is considered in this figure.

We may therefore state that only the acceleration coupling model is able to describe at least qualitatively the main features of VIV at low Skop–Griffin parameter S_G and mass ratio m^*.

4.5. Effective added mass

A consideration valid for all the three coupling models may finally be drawn, concerning the effective added mass exerted on the structure oscillator. In Fig. 8 the phase φ between the structure displacement y and the lift q is observed to jump of π passing through the lock-in domain. This qualitatively models the changes of vortex timing, lift force phase and then the sign of the lift force in phase with the structure acceleration, referred to as an effective added mass in the literature (Khalak and Williamson, 1999). All this has already been observed experimentally for forced (Carberry et al.,

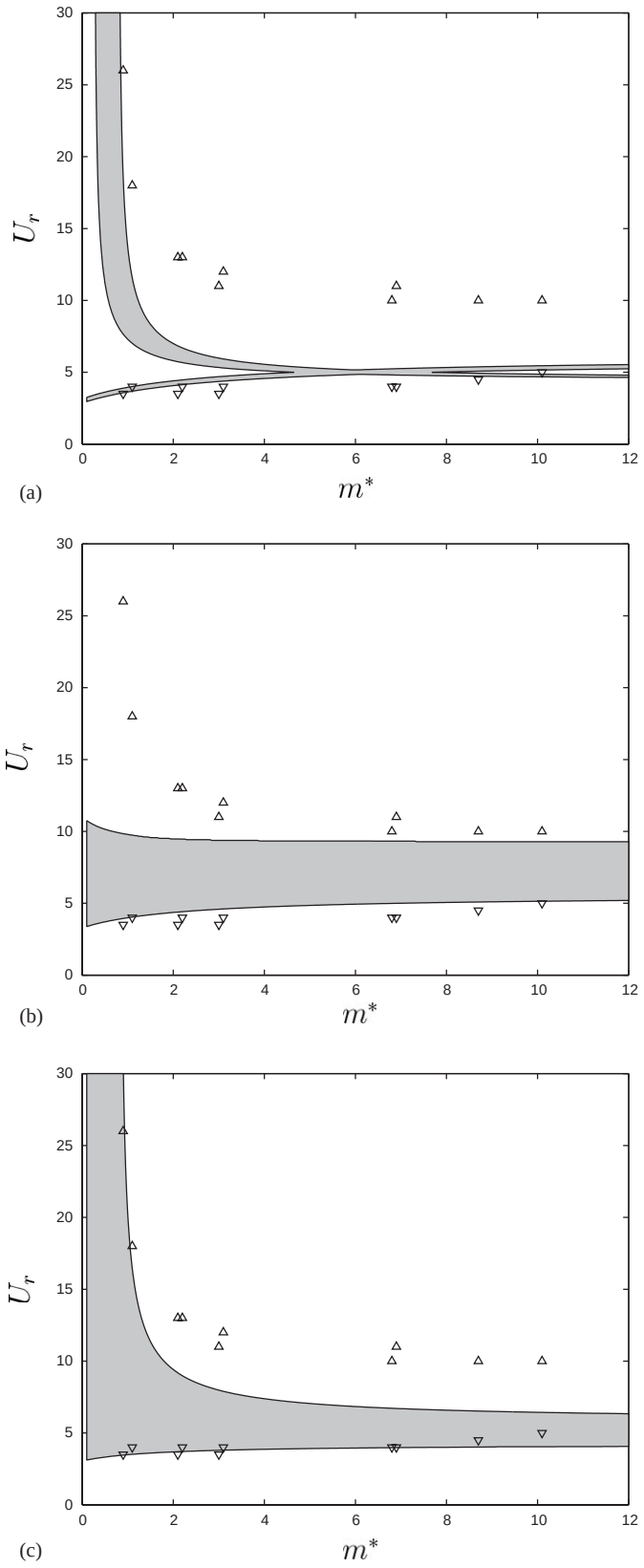

Fig. 10. Lock-in domains as a function of the mass ratio m^* at low $S_G = 0.01$: (a) displacement model; (b) velocity model; (c) acceleration model. Experimental data from Govardhan and Williamson (2000): ∇, lower lock-in bound; $\triangle$, upper lock-in bound.

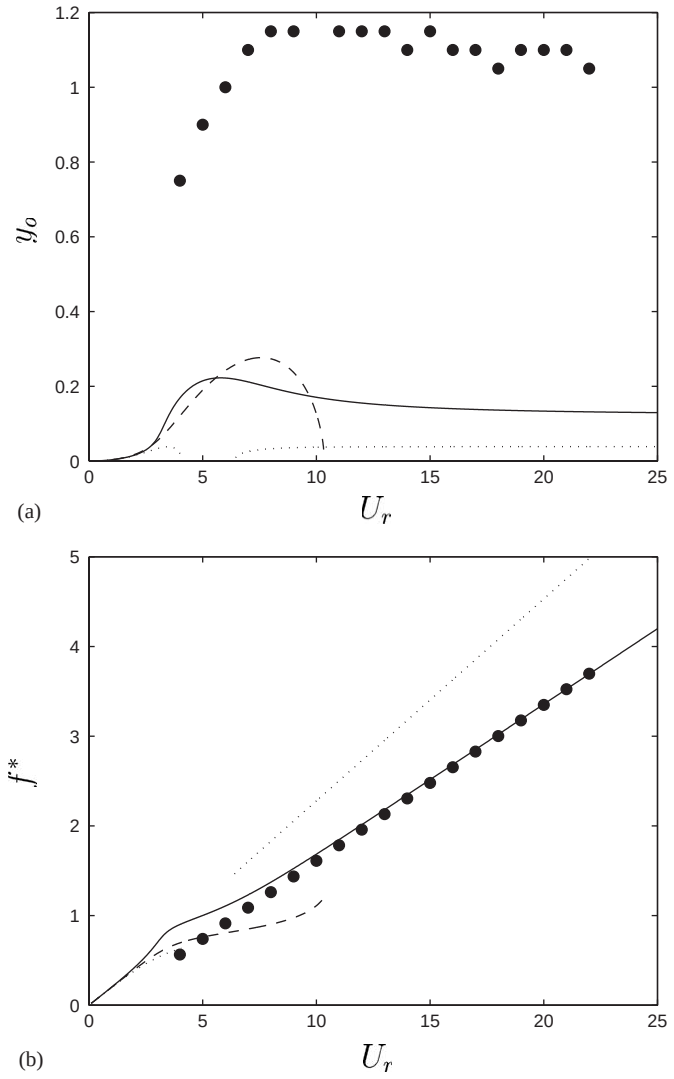

Fig. 11. Response at low mass ratio $m^* = 0.52$ and low reduced damping $\xi = 0.0052$: (a) Oscillation amplitude; (b) Angular frequency. Experimental data: •, Govardhan and Williamson (2000). Present coupled models: ⋯, displacement; - -, velocity; —, acceleration.

2001) and free vibrations (Govardhan and Williamson, 2000), and also simulated by 2-D, CFD (Lu and Dalton, 1996; Blackburn and Henderson, 1999). As described in Section 3, at low U_r vortices are shed at the structure peak displacement on the external side and the fluctuating lift force is in-phase with respect to the structure displacement, leading to a positive effective added mass. Conversely, at high U_r vortices are shed at the structure peak displacement on the internal side and q, y are then out-of-phase, leading to a negative effective added mass. In the structure oscillator (6), the added mass deriving from the fluctuating lift force in phase with the structure acceleration reads

$$C_A = \frac{C_{Lo}}{4\pi^3\,\mathrm{St}^2\,M}(\delta^2 - \omega^2) \tag{38}$$

and depends on the particular coupling model through the value of ω as a function of U_r, Eq. (25), see Fig. 5. The so-called effective added mass coefficient $C_M + C_A$ is plotted in Fig. 12 as a function of U_r: the three coupling models give similar results, in good agreement with experimental data from Vikestad et al. (2000).

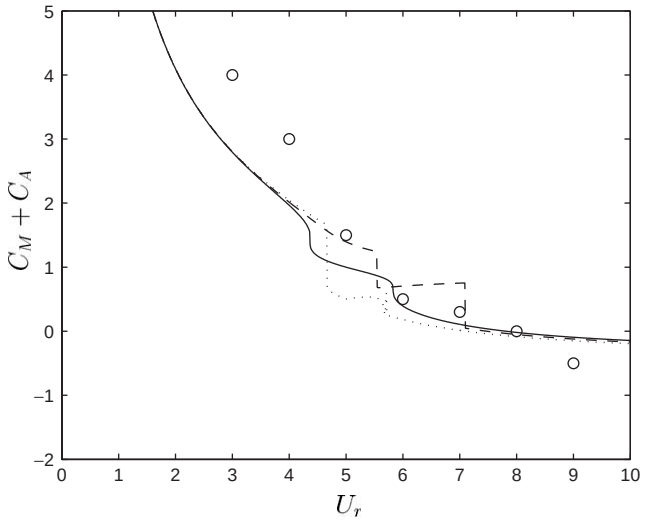

Fig. 12. Effective added mass at $M = 0.002, \xi = 0.01$. Experimental data: ○, Vikestad et al. (2000). Present coupled models: ⋯, displacement; - -, velocity; —, acceleration.

5. Discussion

Within a class of low-order models based on a van der Pol wake oscillator, three coupling models have been systematically examined and compared in terms of their ability to describe, qualitatively and quantitatively, the main phenomena observed in 2-D VIV. The first two models, referred to as displacement and velocity coupling, have been partially analyzed before in the literature, while the third, referred to as acceleration coupling, is a new model. The acceleration coupling model is shown to perform noticeably better than both the velocity and displacement coupling models.

A physical insight for the effectiveness of the acceleration coupling in modelling VIV may be offered by the following kinematic considerations: (a) a static transverse displacement y of the structure in a uniform flow does not modify the fluctuating nature of the near wake, and therefore the coupling should not depend on y; (b) a transverse displacement of the structure at a constant velocity $\dot{y}$ only changes the angle of attack of the flow. This affects the hydrodynamic damping resulting from the drag, already taken into account in through the parameter γ (Blevins, 1990), but leaves unchanged the lift fluctuations, and therefore the coupling should not depend on $\dot{y}$; (c) finally, only the structure acceleration $\ddot{y}$ is expected to affect the wake dynamics. Some parallel may be drawn with the case of a mass–spring oscillator subject to base oscillations, which is equivalent to an inertial excitation in the relative frame moving with the support. We may consider here the near wake as a van der Pol oscillator attached to the moving structure.

Another interesting observation comes from energy considerations. The near wake variable q being directly related to the lift coefficient C_L, the energy transfer from the wake to the structure is expressed by $\int q\dot{y}\,\mathrm{d}t$. In the freely oscillating coupled system, a positive energy transfer is assured by the phase condition $0 \ll -\varphi/\pi \ll 1$, which is satisfied by all the three coupling models for all reduced velocities. This unidirectional energy flow is a necessary condition for free vibrations to occur. Moreover, for forced oscillations the corresponding phase condition $0 \ll \psi/\pi \ll 1$ is satisfied only by the acceleration coupling model and, for $U_r \gg 1/\mathrm{St}$, by the velocity coupling model. Thus, only for these cases significant free structure oscillations and near wake fluctuations may occur simultaneously, whereas for the displacement coupling model, weak structure oscillations are allowed only by a decrease in the wake fluctuation amplitude.

The dynamics of the three coupling models have been analyzed (Section 4) upon the choice of common values of all parameters, and particularly the van der Pol parameter ε and the coupling force scaling A (Section 3). In this approach, we have chosen to estimate the near wake parameters ε and A from experimental data on forced vortex shedding only, so that only the dynamics of the near wake is involved, as these parameters are related to the intrinsic wake dynamics. Note that these parameters may also have been estimated by considering experimental data on free VIV, i.e., from Griffin plots and lock-in diagrams. This would allow a better fit on the structure oscillation amplitude, but a degraded fit on the dynamics of forced wakes, Fig. 9, as the corresponding value of A/ε would be higher.

It should also be reminded that the values of ε and A have been fixed comparing the vortex lift force to experimental data on the total lift force, namely under the approximation $C_L^{\mathrm{tot}} \sim C_L$, in order to allow a comparison between the

different coupling models. For the acceleration coupling model, the fit of experimental data in Figs. 2 and 3 may be done using the total lift magnification K^{tot} instead of the lift magnification K, Eq. (19). At the basic resonance state, from Eq. (19) we have $K^{\text{tot}} > K$, which would lead to a smaller ratio of A/ε, say $A/\varepsilon = 10$. Note that while the lock-in domain associated to K is clearly asymmetric with respect to $U_r = 1/\text{St}$, Fig. 3c, that of K^{tot} would be symmetric. Nevertheless, this leaves almost unchanged ε, yielding $\varepsilon = 0.3$.

6. Conclusions

Considering a wake oscillator coupled with a structure oscillator, we have analyzed the ability of generic forms of coupling to qualitatively and quantitatively describe the main phenomena observed in 2-D VIV. This has been done by first estimating the values of all parameters from comparison with experimental data on forced vortex shedding (Section 3), then by deriving analytical and numerical results on the fully coupled system (Section 4). These results have been systematically compared with experimental data from the literature such as oscillation amplitude at lock-in, extension of lock-in and effective added mass. The following conclusions may be drawn from this analysis:

(a) The displacement coupling fails in modeling the lift phase in forced vortex shedding, the lift magnification at lock-in and all VIV features at low S_G numbers.
(b) The velocity coupling fails in modelling the lift phase in forced vortex shedding and the range of lock-in at low S_G numbers.
(c) The acceleration coupling succeeds in modeling all features of VIV analyzed in this paper, qualitatively and, in some aspects, quantitatively.

The recommended coupled model reads, in dimensional form

$$\begin{aligned} &\left(m_s + \tfrac{1}{4}\pi C_M \rho D^2\right)\ddot{Y} + [r_s + \gamma 2\pi \text{St}(U/D)\rho D^2]\dot{Y} + hY = \tfrac{1}{4}\rho U^2 D C_{Lo} q, \\ &\ddot{q} + \varepsilon[2\pi \text{St}(U/D)](q^2 - 1)\dot{q} + [2\pi\,\text{St}\,(U/D)]^2 q = (A/D)\ddot{Y}, \end{aligned} \tag{39}$$

where the parameters $C_M, \text{St}, \gamma, C_{Lo}, \varepsilon, A$ fix the system dynamics following closed form relations.

Because of its simplicity, the van der Pol wake oscillator model may be easily extended to other 2-D and 3-D aspects of vortex shedding and vortex-induced vibrations. It has been shown to be able to model VIV of two cylinders in tandem arrangement (Facchinetti et al., 2002a), cellular vortex shedding in shear flow (Balasubramanian and Skop, 1996; Facchinetti et al., 2002b), suppression of vortex shedding behind sinuous cylinders (Facchinetti et al., 2002b), and vortex-induced waves along cables (Facchinetti et al., 2001, 2002c, d). Such a model becomes really useful when computational limits arise for flow-field numerical simulations, particularly for 3-D domains with large aspect ratio and at high Reynolds numbers. Moreover, phenomenological models based on wake oscillators allow accessible analytical considerations and thus help the understanding of the physics of VIV.

References

Albarède, P., Provansal, M., 1995. Quasi-periodic cylinder wakes and the Ginzurg-Landau model. Journal of Fluid Mechanics 291, 191–222.

Balasubramanian, S., Skop, R.A., 1996. A nonlinear oscillator model for vortex shedding from cylinders and cones in uniform and shear flows. Journal of Fluids and Structures 10, 197–214.

Balasubramanian, S., Skop, R.A., 1997. A new twist on an old model for vortex-excited vibrations. Journal of Fluids and Structures 11, 395–412.

Balasubramanian, S., Skop, R.A., Haan, F.L., Szewczyk, A.A., 2000. Vortex-excited vibrations of uniform pivoted cylinders in uniform and shear flow. Journal of Fluids and Structures 14, 65–85.

Bearman, P.W., 1984. Vortex shedding from oscillating bluff bodies. Annual Review of Fluid Mechanics 16, 195–222.

Birkoff, G., Zarantanello, E.H., 1957. Jets, Wakes and Cavities. Academic Press, New York.

Bishop, R.E.D., Hassan, A.Y., 1964. The lift and drag forces on a circular cylinder oscillating in a flowing fluid. Proceedings of the Royal Society of London A 277, 51–75.

Blackburn, H.M., Henderson, R.D., 1999. A study of two-dimensional flow past an oscillating cylinder. Journal of Fluid Mechanics 385, 255–286.

Blevins, R.D., 1990. Flow-Induced Vibrations. Van Nostrand Reinhold, New York.

Carberry, J., Sheridan, J., Rockwell, D., 2001. Forces and wake modes of an oscillating cylinder. Journal of Fluids and Structures 15, 523–532.

Facchinetti, M.L., de Langre, E., Biolley, F., 2001. Vortex-induced waves along cables. Bulletin of the American Physical Society 46, 128.

Facchinetti, M.L., de Langre, E., Fontaine, E., Bonnet, P.A., Etienne, S., Biolley, F., 2002a. VIV of two cylinders in tandem arrangement: analytical and numerical modeling. In: Proceedings of the 12th International Offshore and Polar Engineering Conference, Kitakyushu, Japan, 02-JRC-05, pp. 524–531.

Facchinetti, M.L., de Langre, E., Biolley, F., 2002b. Vortex shedding modeling using diffusive van der Pol oscillators. Comptes Rendus Mécanique 330, 451–456.

Facchinetti, M.L., de Langre, E., Biolley, F., 2002c. Vortex-induced waves along cables. In: Proceedings of the Fifth Symposium on Fluid–Structure Interactions, Aeroelasticity, Flow-Induced Vibrations and Noise IMECE2002-32161. Also European Journal of Mechanics B/Fluids 2004, in press.

Facchinetti, M.L., de Langre, E., Biolley, F., 2002d. Experiments on vortex-induced traveling waves along a cable. Proceedings of the Third Conference on Bluff Body Wakes and Vortex-Induced Vibrations, Port-Douglas, Australia, pp. 215–217.

Govardhan, R., Williamson, C.H.K., 2000. Modes of vortex formation and frequency response of a freely vibrating cylinder. Journal of Fluid Mechanics 420, 85–130.

Griffin, O.M., 1980. Vortex-excited cross flow vibrations of a single cylindrical tube. ASME Journal of Pressure Vessel Technology 102, 158–166.

Hartlen, R.T., Currie, I.G., 1970. Lift-oscillator model of vortex-induced vibration. Journal of the Engineering Mechanics Division EM5, 577–591.

Khalak, A., Williamson, C.H.K., 1999. Motions, forces and mode transitions in vortex-induced vibrations at low mass-damping. Journal of Fluids and Structures 13, 813–851.

Kim, W.J., Perkins, N.C., 2002. Two-dimensional vortex-induced vibration of cable suspensions. Journal of Fluids and Structures 16, 229–245.

King, R., 1977. Vortex excited oscillations of yawed circular cylinders. Journal of Fluid Engineering 99, 495–502.

Krenk, S., Nielsen, S.R.K., 1999. Energy balanced double oscillator model for vortex-induced vibrations. ASCE Journal of Engineering Mechanics 125, 263–271.

Landl, R., 1975. A mathematical model for vortex-excited vibrations of bluff bodies. Journal of Sound and Vibration 42, 219–234.

Leonard, A., Roshko, A., 2001. Aspects of flow-induced vibrations. Journal of Fluids and Structures 15, 415–425.

Lu, X.Y., Dalton, C., 1996. Calculation of the timing of vortex formation from an oscillating cylinder. Journal of Fluids and Structures 10, 527–541.

Lucor, D., Imas, L., Karniadakis, G.E., 2001. Vortex dislocations and force distribution of long flexible cylinders subjected to sheared flows. Journal of Fluids and Structures 15, 641–650.

Monkewitz, P.A., Williamson, C.H.K., Miller, G.D., 1996. Phase dynamics of Karman vortices in cylinder wakes. Physics of Fluids 8, 91–96.

Mureithi, N.W., Kanki, H., Nakamura, T., 2000. Bifurcation and perturbation analysis of some vortex shedding models. In: Proceedings of the Seventh International Conference on Flow-Induced Vibrations, Luzern, Switzerland. Balkema, Rotterdam, pp. 61–68.

Nayfeh, A.H., 1993. Introduction to Perturbation Techniques. Wiley, New York.

Noack, B.R., Ohle, F., Eckelman, H., 1991. On cell formation in vortex streets. Journal of Fluid Mechanics 227, 293–308.

Olinger, D.J., 1998. A low-order model for vortex shedding patterns behind vibrating flexible cables. Physics of Fluids 10, 1953–1961.

Pantazopoulos, M.S., 1994. Vortex-induced vibration parameters: critical review. In: Proceedings of the 17th International Conference on Offshore Mechanics and Arctic Engineering, Osaka, Japan, pp.199–255.

Park, D.S., Redekopp, L.G., 1992. A model for pattern selection in wake flows. Physics of Fluids A 4, 1–10.

Parkinson, G., 1989. Phenomena and modeling of flow-induced vibrations of bluff bodies. Progress in Aerospace Sciences 26, 169–224.

Plaschko, P., 2000. Global chaos in flow-induced oscillations of cylinders. Journal of Fluids and Structures 14, 883–893.

Saffman, P.G., 1992. Vortex Dynamics. University Press, Cambridge.

Shiels, D., Leonard, A., Roshko, A., 2001. Flow-induced vibration of a circular cylinder at limiting structural parameters. Journal of Fluids and Structures 15, 3–21.

Skop, R.A., Luo, G., 2001. An inverse-direct method for predicting the vortex-induced vibrations of cylinders in uniform and nonuniform flows. Journal of Fluids and Structures 15, 867–884.

Skop, R.A., Griffin, O.M., Koopman, G.H., 1973. The vortex-excited resonant vibrations of circular cylinders. Journal of Sound and Vibration 31, 235–249.

Stansby, P.K., 1976. The locking-on of vortex shedding due to the cross-stream vibration of circular cylinders in uniform and shear flows. Journal of Fluid Mechanics 74, 641–665.

Vickery, B.J., Watkins, R.D., 1962. Flow-induced vibration of cylindrical structures. In: Proceedings of the First Australian Conference, University of Western Australia, pp. 213–241.

Vikestad, K., Vandiver, J.K., Larsen, C.M., 2000. Added mass and oscillation frequency for a circular cylinder subjected to vortex-induced vibrations and external disturbance. Journal of Fluids and Structures 14, 1071–1088.